

The Effect of Multiple Ion Substitutions on Halide Ion Migration in Perovskite Solar Cells

Samuel R. Pering^{1*†}, Petra J. Cameron¹

1. Department of Chemistry, University of Bath, Bath BA2 7AY, UK

† Samuel R. Pering current address: Department of Materials, Loughborough University, LE11 3TU, UK

SUPPORTING INFORMATION

METHODS:

PEROVSKITE PRECURSOR SYNTHESIS:

FAPbI₃ perovskites were made using a 1.25:1.25 molar ratio of formamidinium iodide (FAI, Greatcell Solar) and PbI₂ (Sigma, 99 %) in a solution using a solvent ratio of 4:1 DMF:DMSO. For the substituted perovskites, precursor solutions for the triple-cation perovskite were made using the proportions and methods reported by Saliba *et al.*¹

All films were deposited at 5000 rpm for 30 seconds, with an ethyl acetate antisolvent being used 15 seconds into the spin-coating method. Films were annealed at 150 °C unless otherwise stated.

DEVICE FABRICATION

Either Fluorine doped Tin Oxide glass (FTO) (Solaronix, unless otherwise specified) with a sheet resistance of 15 Ω/square or microscope glass (VWR) was used. For film measurements, the glass was used as purchased. Glass was cut to 25 mm × 25 mm pieces. For Solar Cell fabrication a 5 mm strip was etched from the middle of the glass using 2 M HCl (Sigma) and Zn powder (Sigma) before the cleaning step.

Glass was cleaned in an ultrasonic bath at a temperature of 80 °C using the following solvents: 2 % Hellmanex in MilliQ water, water, acetone, isopropanol and ethanol. Following the final step the glass was dried using N₂ gas and placed in a UV/Ozone cleaner for 20 minutes.

The HTM solution contained 50 mgmL⁻¹ Nickel(II) acetate hexahydrate (Sigma, 99.998 %) in 2-methoxy ethanol (Sigma, 99.8 %). 12 μL ethanolamine (Sigma, 98 %) was added to this solution, and it was filtered before use. Films were deposited at 3000 rpm for 30 seconds and annealed at 500 °C for 30 minutes.

A 1.25:1.25 M solution of MAI and PbI₂ was dissolved in a 4:1 mixture of DMF and DMSO at 50 °C – also filtered before use. Perovskite films were formed by spin-coating at 4000 rpm for 30 seconds. Ethyl acetate (Sigma, 99.8 %) was used as the antisolvent, deposited 6 seconds into the spin-coating process. Films were left to anneal at 100 °C for 15 minutes.

After cooling, a solution of 20 mgmL⁻¹ PC₇₁BM (Ossila, 95 %) in chlorobenzene was filtered, and deposited onto the perovskite films for 30 seconds at 3000 rpm. A final spin-coating step used a solution of 0.5 mgmL⁻¹ bathocuproine (Sigma, 96 %) in ethanol, deposited at 6000 rpm for 30 seconds.

A 60 nm silver (Alfa Aesar) contact was deposited by thermal evaporation.

ANALYSIS:

Crystallography: A Bruker axis D8 advance powder x-ray diffractometer with a Cu K α source and Ge monochromator was used for Powder/Thin film X-ray diffraction. Measurements were taken from 2 θ values of 5 ° to 80 °.

UV/Vis Spectroscopy: Thin film optical Transmission and Reflectance measurements were performed on a PerkinElmer Lambda 750S UV/Vis spectrometer, from 1000 nm to 250 nm. Absorption was calculated as incident light – (transmission + reflectance).

Atomic Force Microscopy: AFM images were taken on a Nanosurf easyscan 2 FlexAFM system in dynamic mode using a force of 20 nN. A ContAl0F Tip was used for measurements.

JV Curves: Current density-voltage curves were measured using a 2400 series Sourcemeter (Keithley Instruments), under simulated AM1.5 sunlight at 100 mW cm⁻² irradiance generated using a class AAA solar simulator (TS-Space Systems) at room temperature in air. The intensity was calibrated using a certified silicon reference cell (Fraunhofer). The active area of the pixels was 0.0625 cm², measured using a mask of the same area. Voltage scans were taken from 1.1 V (preconditioning time 5s) to 0 V at 100 mVs⁻¹. Measurements were taken in air at room temperature. *Error Analysis:* Solar simulator calibrated to within accepted range for reference cell current density – potential systematic error of ± 0.5 mAcm⁻² (max 3% error based on lowest mean current density).

Electrochemical Impedance Spectroscopy: EIS measurements were taken on a Solartron Modulab, measurements were taken in air under 73 mW cm⁻² illumination at open circuit between 1MHz and 5mHz with a 10 mV perturbation. A 560 nm blue LED was used as the illumination source. The temperature of the cell was controlled by a Peltier element. Devices were measured within 1 day of fabrication. *Error Analysis:* Temperature of Peltier element correct to 4 decimal places. Errors from calculations based on fitting provided in data. Random error – connections of solar cell to potentiostat.

SUPPLEMENTARY FIGURES

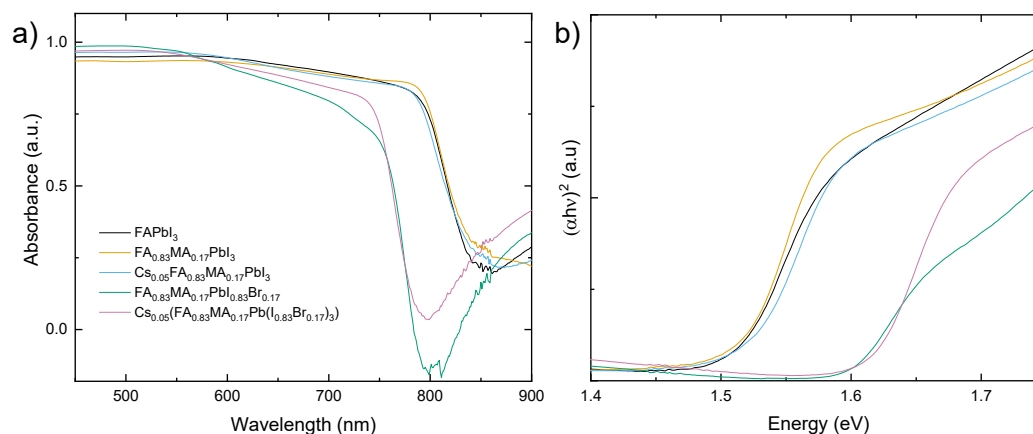


Figure S1. UV/Vis spectroscopy of the perovskite materials investigated through this study: a) absorbance and b) Tauc plot

Table S1. Average PSC parameters (with standard deviation over at least 15 pixels)

Perovskite	Voltage (V)	Current Density (mAcm ⁻²)	Fill Factor (%)	Efficiency (%)	Champion Cell Efficiency (%)
FAPbI ₃	0.78 ± 0.01	16.31 ± 1.24	62.50 ± 7.90	7.90 ± 1.08	9.58
FA _{0.83} MA _{0.17} PbI ₃	0.95 ± 0.04	18.16 ± 1.22	62.23 ± 3.18	10.76 ± 1.15	11.40
Cs _{0.05} (FA _{0.83} MA _{0.17}) _{0.95} PbI ₃	0.85 ± 0.01	17.41 ± 1.65	57.79 ± 2.65	8.53 ± 0.88	10.16
FA _{0.83} MA _{0.17} Pb(I _{0.83} Br _{0.17}) ₃	1.01 ± 0.04	16.72 ± 1.51	52.41 ± 4.42	8.80 ± 0.88	10.10
Cs _{0.05} (MA _{0.17} FA _{0.83}) _(0.95) Pb(I _{0.83} Br _{0.17}) ₃	0.97 ± 0.04	15.51 ± 1.81	60.06 ± 4.07	8.99 ± 1.13	11.00

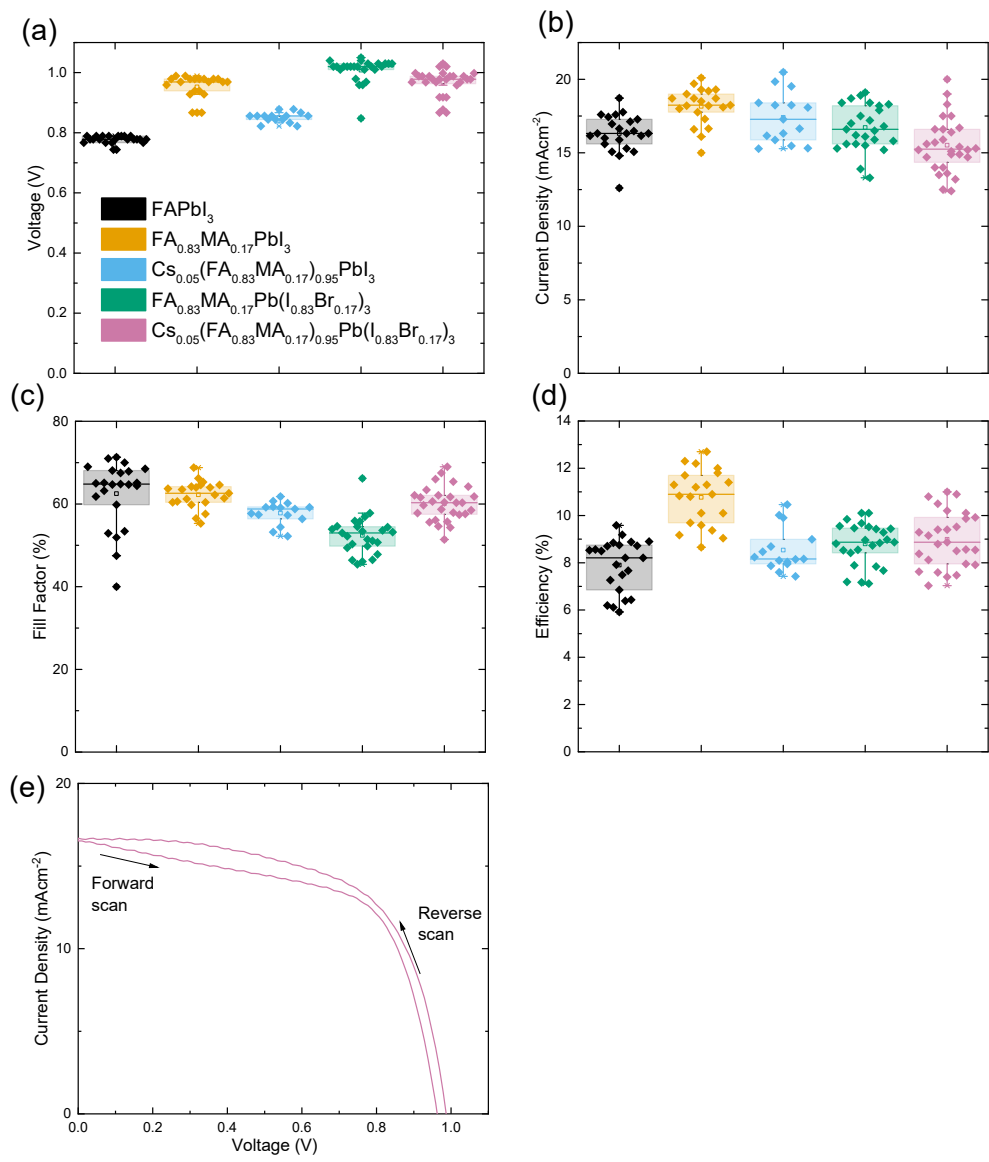


Figure S2. Box plots for VOC, JSC, Fill factor and efficiency for the cells, and e) JV curve for representative Cs_{0.05}(MA_{0.17}FA_{0.83})_{0.95}Pb(I_{0.83}Br_{0.17})₃ device

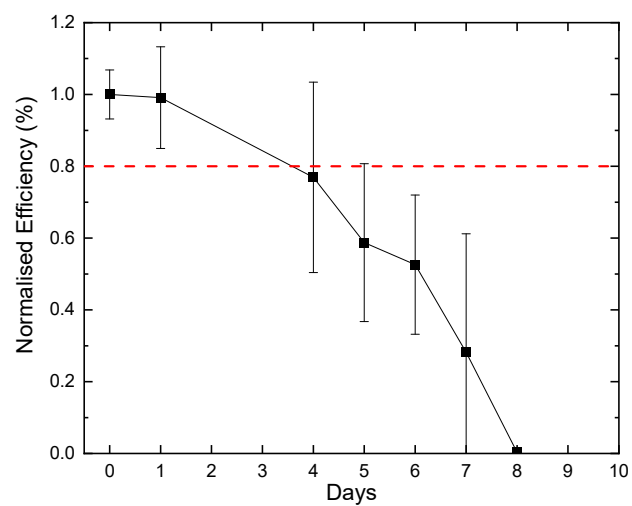


Figure S3. Normalised Photovoltaic stability of Formamidinium Lead Iodide, average over 6 pixels. Dashed line representing 80% efficiency. All cells were measured for impedance within 1 day of first PV measurement.

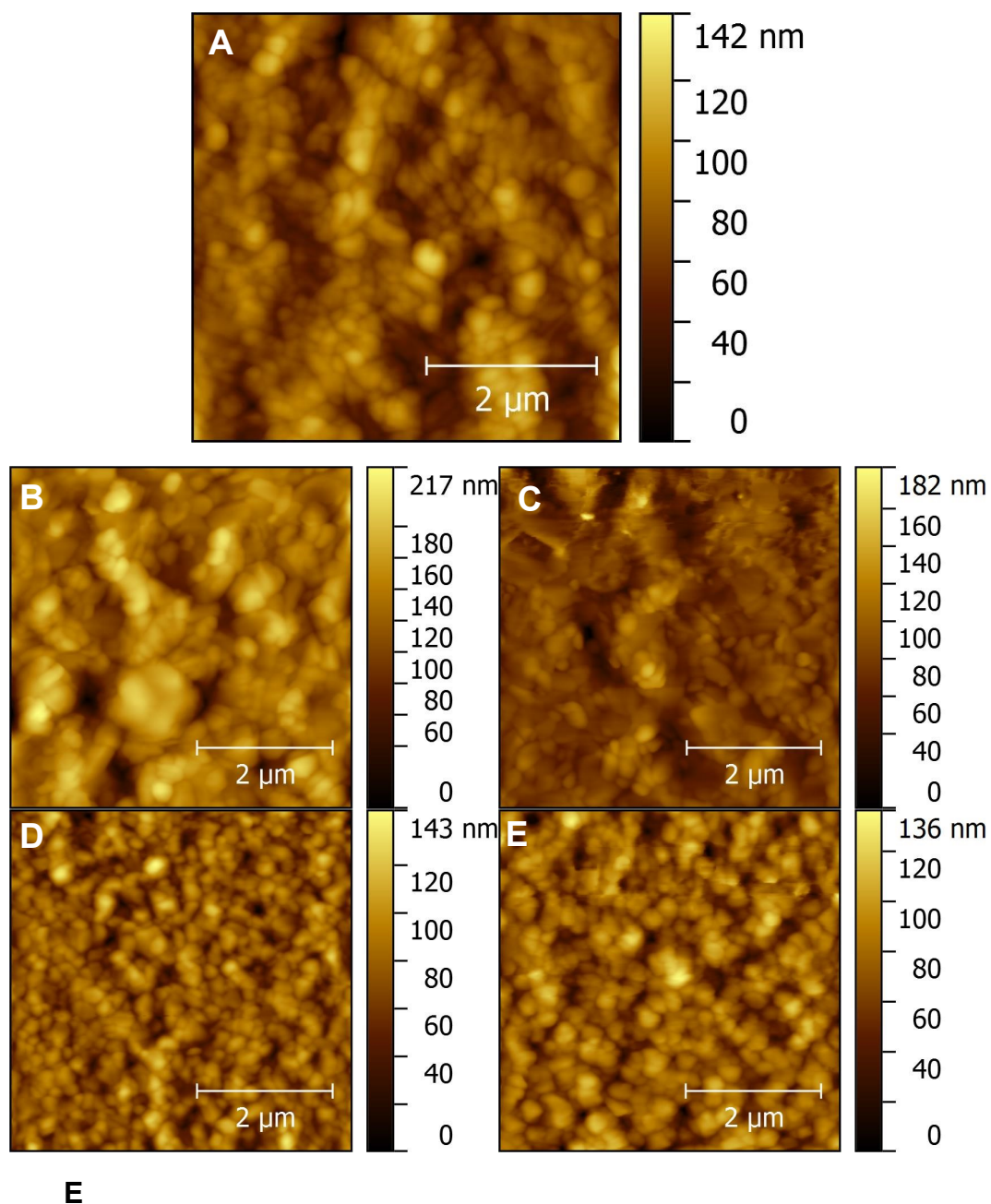


Figure S4. AFM images of **a)** FAPbI_3 , **b)** $\text{FA}_{0.83}\text{MA}_{0.17}\text{PbI}_3$, **c)** $\text{Cs}_{0.05}(\text{FA}_{0.83}\text{MA}_{0.17})_{0.95}\text{PbI}_3$, **d)** $\text{FA}_{0.83}\text{MA}_{0.17}\text{Pb}(\text{I}_{0.83}\text{Br}_{0.17})_3$ and **e)** $\text{Cs}_{0.05}(\text{MA}_{0.17}\text{FA}_{0.83})_{0.95}\text{Pb}(\text{I}_{0.83}\text{Br}_{0.17})_3$

Table S2. Lattice parameter (a) and hydrogen bond length for a series of lead-halide based perovskite materials

Material	Structure	Lattice parameter a, (Å)	Hydrogen bond length (Å)	Tolerance Factor	Notes	Ref.	
MAPbI ₃	Tetragonal	-	3.15-3.18	0.95	Computational	2	
	Orthorhombic	-	2.61-2.81			2	
	Cubic	-	3.12-3.52			2	
	Tetragonal	6.30	-			3	
	Tetragonal	6.28	2.6			4	
			(average)				
MA _{0.75} FA _{0.25} PbI ₃	Cubic	6.30	2.6 (MA)		Computational and average values	4	
			2.8 (FA)			4	
MA _{0.25} FA _{0.75} PbI ₃	Cubic	6.33	2.6 (MA)			4	
			2.7 (FA)				
MA _{0.2} FA _{0.8} PbI ₃	-	6.34	-			3	
FAPbI ₃	Cubic	6.36		1.04		3	
	Cubic	6.36	2.75-3.0			5	
	Cubic	6.34	2.7		Computational	4	
Cs _{0.15} FA _{0.85} PbI ₃	Cubic	-	2.65-2.75		Computational	6	
CsPbI ₃	Cubic	6.29	-	0.89	High Temperature measurement	7	
FAPbI ₃ -MABr	Cubic	6.31				8	
MAPbBr ₃	Cubic	5.90		0.99		9	
	-	8.44				High pressure measurement	10
	-	8.46	2.8-3.0			Tilted structure	11
FAPbBr ₃	Cubic	-	2.4		Thin-film	12	
CsPbBr ₃	Cubic		2.4		Thin-film	12	
	Cubic	5.87			Computational	13	

Electrochemical Impedance Spectroscopy Figures:

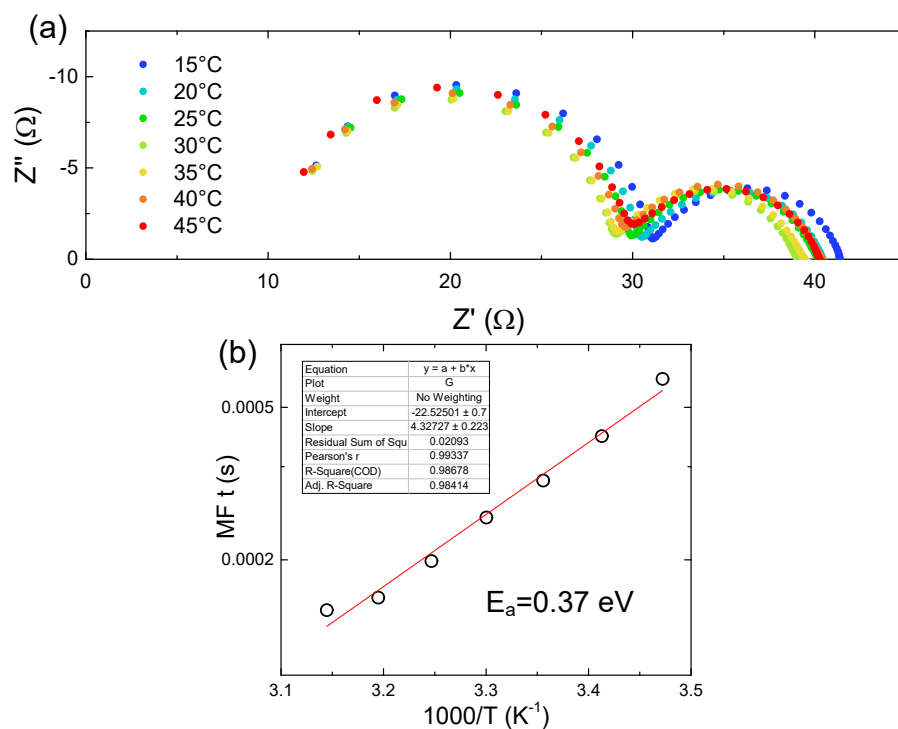


Figure S5. The change in FAPI impedance with temperature: a) Nyquist plots, b) Arrhenius plot for the mid-frequency feature with inset example of error for activation energy calculations

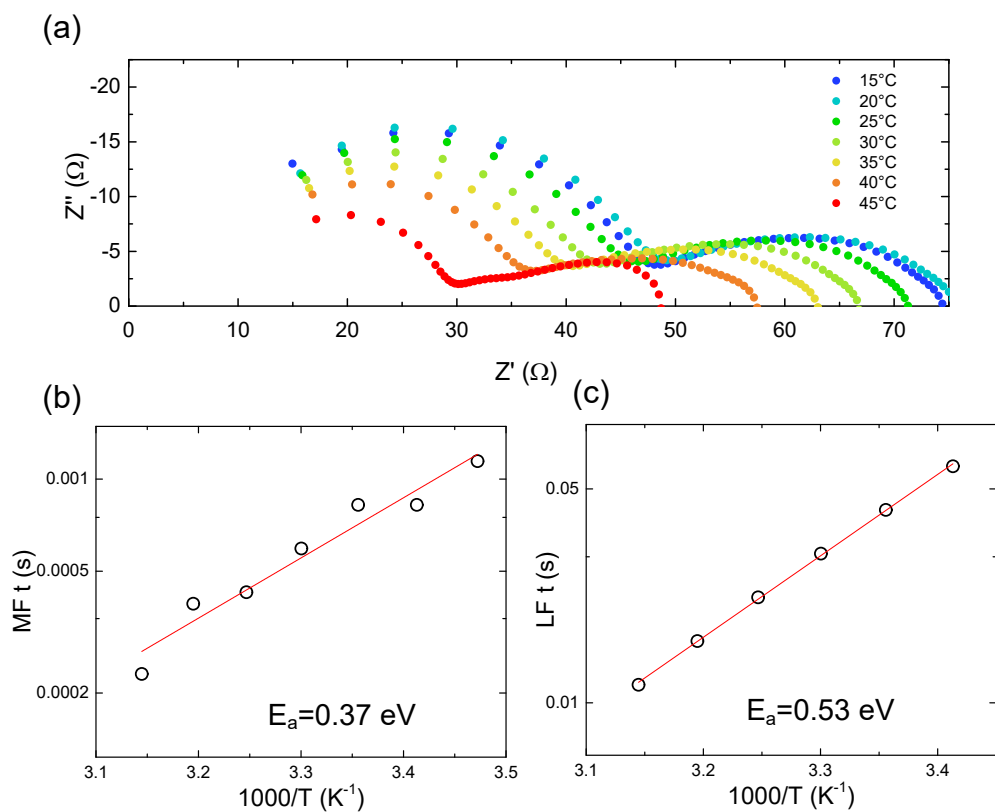


Figure S6. The change in $FA_{0.83}MA_{0.17}PbI_3$ impedance with temperature: a) Nyquist plots, b) Arrhenius plot for the mid-frequency feature and c) for the low frequency feature.

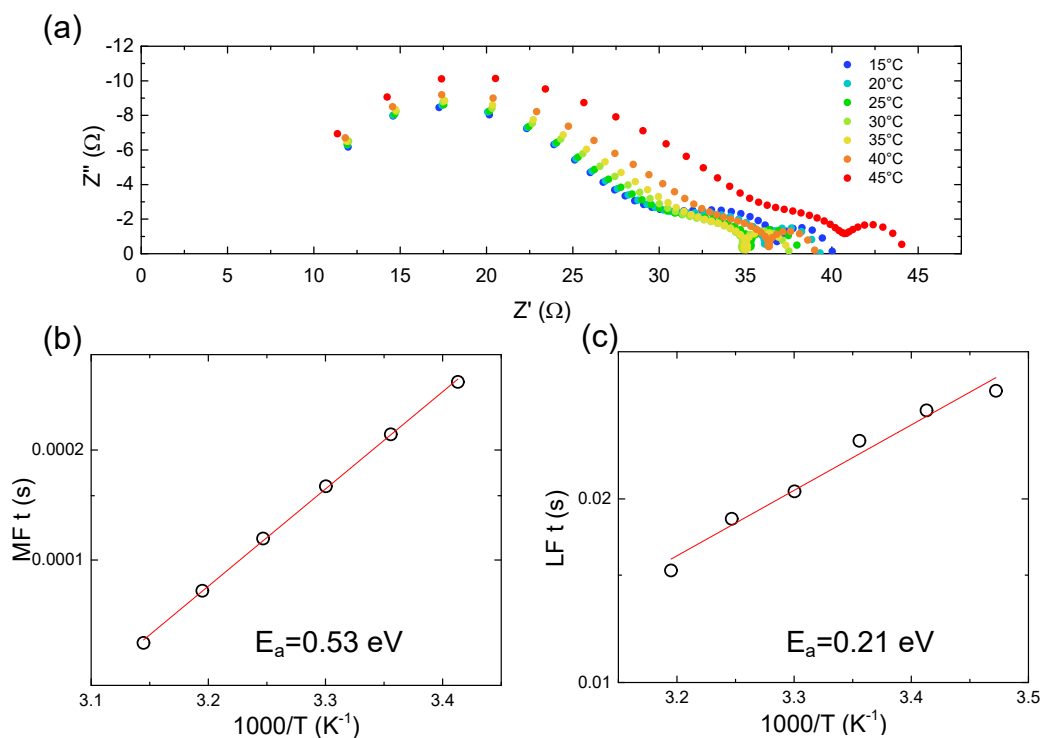


Figure S7. The change in $Cs_{0.05}(FA_{0.83}MA_{0.17})_{0.95}PbI_3$ impedance with temperature: a) Nyquist plots, b) Arrhenius plot for the mid-frequency feature and c) for the low frequency feature.

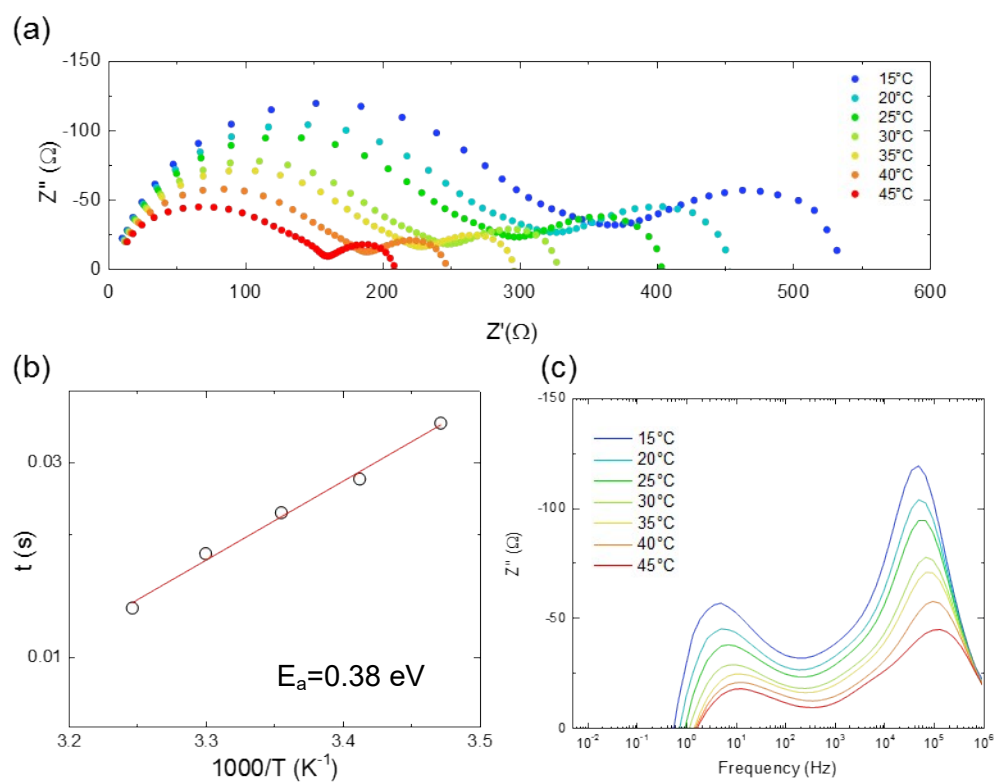


Figure S8. The change in $\text{FA}_{0.83}\text{MA}_{0.17}\text{Pb}(\text{I}_{0.83}\text{Br}_{0.17})_3$ impedance with temperature: a) Nyquist plots, b) Arrhenius plot for the second semicircle and c) Cole plot

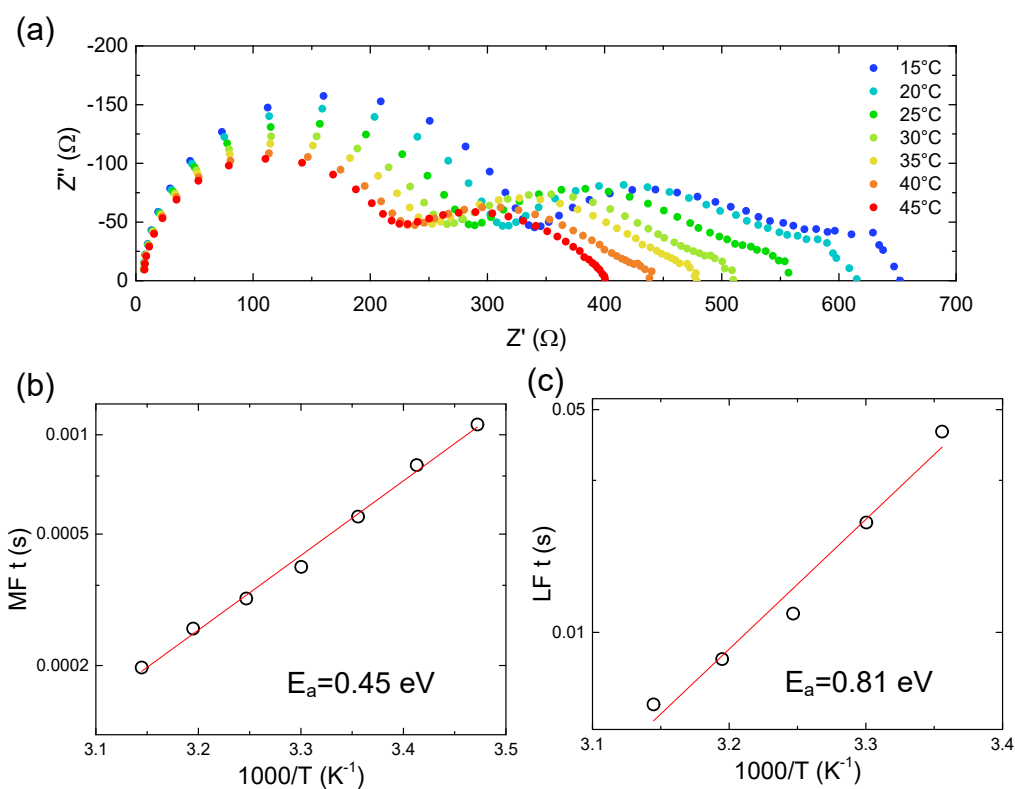


Figure S9. The change in $\text{Cs}_{0.05}((\text{FA}_{0.83}\text{MA}_{0.17})_{0.95}\text{Pb}(\text{I}_{0.83}\text{Br}_{0.17})_3)$ impedance with temperature: a) Nyquist plots and b) Arrhenius plot for the low frequency semicircle

Table S3. Data for octahedral-corrected tolerance factor¹⁴ (calculated for this work using relative proportions of each ion) and activation energy, including a selection of values from previous work.

Material	Tolerance Factor	Activation Energy	Ref.
FAPbI_3	1.035		This work
$\text{FA}_{0.83}\text{MA}_{0.17}\text{PbI}_3$	1.022	0.55	This work
$\text{Cs}_{0.05}((\text{FA}_{0.83}\text{MA}_{0.17})_{0.95}\text{PbI}_3)$	1.013	0.21	This work
$(\text{FA}_{0.83}\text{MA}_{0.17})_{0.95}\text{Pb}(\text{I}_{0.83}\text{Br}_{0.17})_3$	1.031	0.38	This work
$\text{Cs}_{0.05}((\text{FA}_{0.83}\text{MA}_{0.17})_{0.95}\text{Pb}(\text{I}_{0.83}\text{Br}_{0.17})_3)$	1.022	0.81	This work
MAPbI_3	0.957	0.4	15
$\text{MAPb}(\text{I}_{0.975}\text{Br}_{0.025})_3$	0.958	0.78	16
$\text{MA}_{0.95}\text{DM}_{0.05}\text{PbI}_3$	0.963	0.64	15
$\text{MAPb}(\text{I}_{0.937}\text{Br}_{0.063})_3$	0.959	1.12	16

REFERENCES:

1. M. Saliba, T. Matsui, J.-Y. Seo, K. Domanski, J.-P. Correa-Baena, N. Mohammad K., S. M. Zakeeruddin, W. Tress, A. Abate, A. Hagfeldt, and M. Grätzel, *Energy Environ. Sci.*, 2016, **9**, 1989–1997.

2. M. T. Weller, O. J. Weber, P. F. Henry, A. M. Di Pumpo, and T. C. Hansen, *Chem. Commun.*, 2015, **51**, 4180–4183.
3. O. J. Weber, B. Charles, and M. T. Weller, *J. Mater. Chem. A*, 2016, **4**, 15375–15382.
4. M. Senno and S. Tinte, *Phys. Chem. Chem. Phys.*, 2021, **23**, 7376–7385.
5. M. T. Weller, O. J. Weber, J. M. Frost, and A. Walsh, *J. Phys. Chem Lett.*, 2015, **6**, 3209–3212.
6. D. Ghosh, A. R. Smith, A. B. Walker, and M. S. Islam, *Chem. Mater.*, 2018, **30**, 5194–5204.
7. D. M. Trots and S. V Myagkota, *J. Phys. Chem. Solids*, 2008, **69**, 2520–2526.
8. X. Zheng, C. Wu, S. K. Jha, Z. Li, K. Zhu, and S. Priya, *ACS Energy Lett.*, 2016, **1**, 1014–1020.
9. A. Poglitsch and D. Weber, *J. Chem. Phys.*, 1987, **87**, 6373–6378.
10. Y. Wang, X. Lü, W. Yang, T. Wen, L. Yang, X. Ren, L. Wang, Z. Lin, and Y. Zhao, *J. Am. Chem. Soc.*, 2015, **137**, 11144–11149.
11. D. Wiedemann, J. Breternitz, D. W. Paley, and S. Schorr, *J. Phys. Chem. Lett.*, 2021, **12**, 2358–2362.
12. H. Singh, R. Fei, Y. Rakita, M. Kulbak, D. Cahen, A. M. Rappe, and A. I. Frenkel, *Phys. Rev. B*, 2020, **101**, 54302.
13. C.-J. Yu, U.-H. Ko, S.-G. Hwang, Y.-S. Kim, U.-G. Jong, Y.-H. Kye, and C.-H. Ri, *Phys. Rev. Mater.*, 2020, **4**, 45402.
14. W. Travis, E. N. K. Glover, H. Bronstein, D. O. Scanlon, and R. G. Palgrave, *Chem. Sci.*, 2016, **7**, 4548–4556.
15. D. W. Ferdani, S. R. Pering, D. Ghosh, P. Kubiak, A. B. Walker, S. E. Lewis, A. L. Johnson, P. J. Baker, M. S. Islam, and P. J. Cameron, *Energy Environ. Sci.*, 2019, **12**, 2264–2272.
16. R. García-Rodríguez, D. Ferdani, S. Pering, P. J. Baker, and P. J. Cameron, *J. Mater. Chem. A*, 2019, **7**, 22604–22614.